Hydrodynamic Interactions, Hidden Order, and Emergent Collective Behavior in an Active Bacterial Suspension

C. J. Pierce,[1] H. Wijesinghe,[1] E. Mumper,[2] B. H. Lower,[2] S. K. Lower,[2,3,4] and R. Sooryakumar[1]
[1]Department of Physics, The Ohio State University, Columbus, Ohio 43210, USA
[2]School of Environment and Natural Resources, The Ohio State University, Columbus, Ohio 43210, USA
[3]School of Earth Sciences, The Ohio State University, Columbus, Ohio 43210, USA
[4]Department of Microbial Infection and Immunity, The Ohio State University, Columbus, Ohio 43210, USA

(Received 20 July 2018; revised manuscript received 11 September 2018; published 2 November 2018; corrected 2 May 2019)

Spontaneous self-organization (clustering) in magnetically oriented bacteria arises from attractive pairwise hydrodynamics, which are directly determined through experiment and corroborated by a simple analytical model. Lossless compression algorithms are used to identify the onset of many-body self-organization as a function of experimental tuning parameters. Cluster growth is governed by the interplay between hydrodynamic attraction and magnetic dipole repulsion, leading to logarithmic time dependence of the cluster size. The dynamics of these complex, far-from-equilibrium structures are relevant to broader phenomena in condensed matter, statistical mechanics, and biology.

DOI: 10.1103/PhysRevLett.121.188001

One of the distinguishing characteristics of biological systems is the emergence of order from the interactions of discrete active components operating far from equilibrium. Insights into how these interacting components produce functional structures across many length scales is of fundamental importance in biological systems, from collections of eukaryotic cells [1] and bacteria [2], to ant colonies [3] and bird flocks [4]; the phenomena extend to nonbiological active matter such as colloids [5,6] and macroscopic robot swarms [7]. A complete description of these systems requires not only an understanding of the microscopic interactions between components, but also the principles governing the dynamics of the many-body states. In this Letter, we present an experimental and theoretical analysis of both the microscopic hydrodynamic interactions and onset of emergent many-body self-organization in a prototypical active matter system [8,9]—a suspension of motile bacteria.

The bacterial species selected for this study (*Magnetotacticum magneticum* AMB-1 [10]) is chosen for its innate magnetism, which renders it amenable to direct external control [11–15], allowing systematic imposition of orientational coherence on the population. Furthermore, the species is motile—the chemically powered flagellum (a thin helical appendage responsible for cellular propulsion) provides the source of activity. This attribute gives rise to attractive hydrodynamic interactions between cells that produce self-organized states (clusters).

To quantify the pairwise hydrodynamic interactions between two cells, a dilute suspension of AMB-1 is placed in a fluid cell and subjected to an external field ($H_z < 100$ G) oriented perpendicular to the surface, using a previously described system [15,16]. As the cells encounter the surface, they either swim in circular planar orbits stabilized by hydrodynamic effects [17], or align normal to the surface and execute a lateral random walk (in a magnetically stabilized state) [15]. Pairs of cells in this latter state experience attractive hydrodynamic interactions and rotate about their center of mass [18] [Figs. 1(c) and 1(e), inset and the videos S1 and S2 in Supplemental Material [19]]. To determine the spatial dependence of these interactions, a pair of AMB-1 cells is isolated in the fluid cell, far from other cells. The pair is perpendicularly oriented under constant H_z [Fig. 1(a)] causing them to approach one another and form a stably rotating doublet. Once the cells have been brought together, the fields are removed (randomizing cell positions) or tilted (navigating cells along diverging paths [15]). When separated by the desired distance H_z is reapplied and the flow field mediated intercellular interactions return the cells to close contact. This process is repeated until a number (87) of trajectories are compiled, yielding the time of flight (Δt) for the cells to arrive in the doublet configuration (close contact) and angular velocity (ω) as a function of intercellular distance (r), as shown in Figs. 1(c) and 1(e).

We attribute the attractive interaction between cells to Stokeslet ($1/r$) [20] dominated flow fields (the flow arising from a point force) associated with the flagellum. Freely swimming organisms at low Reynolds number (Re) are generally considered to be force and torque free [21]. Hence, the leading order term in the multipole expansion of the flow field is taken to be a Stokeslet dipole. However, a power series fit suggests the presence of lower order terms [Fig. 1(c)], implying that an unpaired force monopole f_m acts on the fluid. The force free condition is then maintained by the balance of the flagellar thrust by the surface.

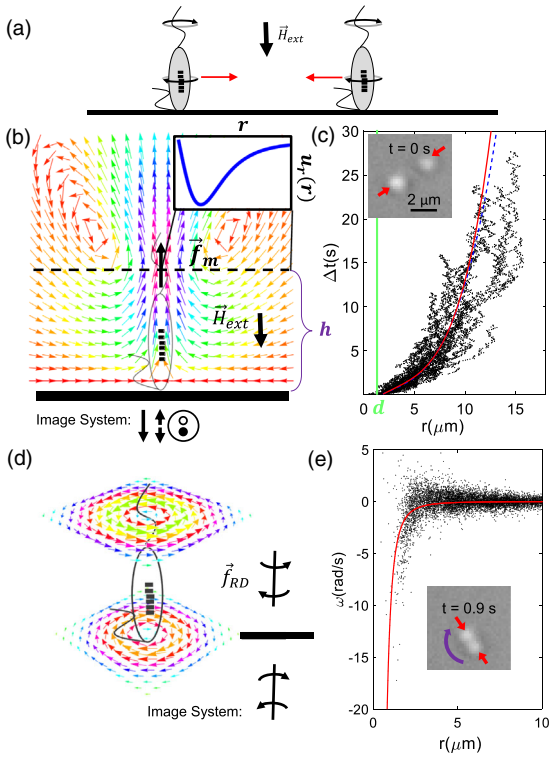

FIG. 1. (a) Schematic of oriented cells and resulting hydrodynamic interaction. (b) Flow field of a pure Stokeslet at height h from a surface with image system (force monopole, force dipole, source dipole). Inset, profile of the velocity [Eq. (1)] derived from the flow field along the dashed line at height h above surface. (c) Time of flight (t) vs intercellular spacing (r) for 87 cellular trajectories from three distinct pairs of cells, along with fit to model (in red) and power series (blue) revealing presence of lower order ($1/r$) terms. Vertical line indicates the minimum cell separation d from fit. Inset, microscopy images of cells forming a rotating doublet. (d) Flow field of a rotlet dipole and image system, along with the singularities. (e) The angular velocity (ω) vs r with fit to rotlet dipole ($1/r^3$) model (red).

We therefore model the cell's flow field using a singularity system comprising a Stokeslet along with its image system [accounting for the surface [22], Fig. 1(b)]. The radial component of the flow velocity $u_r(r)$ in the plane of the singularity, which is assumed to be proportional to the force between the cells, is given by [18,23]

$$u_r(r) = -\frac{f_m}{8\pi\eta}\frac{12h^3 r}{(4h^2+r^2)^{5/2}} = \frac{1}{2}\frac{dr}{dt}, \tag{1}$$

where h is the height of the singularity, dr/dt is the rate of change of the intercellular separation, and η is the dynamic viscosity of water. The time Δt required to travel from an initial separation r to a final closest contact distance d is determined by integrating Eq. (1). Least squares fits to a running average of the data show good agreement and yield reasonable estimates for the three parameters, f_m, d, and h. In particular, a singularity height of $h = 2.6 \pm 0.1$ μm (comparable to average cell length ~ 3 μm [24]), a minimum intercellular spacing of $d = 1.8 \pm 0.2$ μm (agrees with optical image of doublet) and a flagellar thrust $f_m = 0.20 \pm 0.02$ pN (consistent with previous measurements of hydrodynamically analogous species [25–27]) are obtained.

The source of the rotational motion is ascribed to a rotlet dipole field ($\sim 1/r^3$) emanating from the rotating flagellum and counterrotating body [22] [Fig. 1(d)]. The measured angular velocity of the cells about their center of mass along with a fit to a rotlet dipole flow field model [Fig. 1(e)] shows good agreement. The observed clockwise rotation (viewed from above) for all intercellular separations r implies the net rotation of the cell pair is dominated by coupling of the cell body (rather than the flagellum) to the rotlet dipole field. The body has a larger drag coefficient and hence couples more strongly to flow than the flagellum leading to unidirectional motion. The rotation of the flagellum merely attenuates the net effect (rotlet dipole flow field decays as $\omega \sim 1/r^3$, relative to rotlet field $\omega \sim 1/r^2$).

In the many-body case, the attractive hydrodynamic forces result in the formation of clusters, which continually rearrange and rotate under the influence of the rotational effects [Fig. S1(a) and the video S2 in Supplemental Material [19]], analogous to previous observations of spontaneously oriented nonmagnetic bacteria and algae [18,28,29]. The effect of these rotational flows, along with the packing problems created by the spirochete AMB-1 cell morphology [10], prevent the onset of crystalline order within the cluster. Numerical simulation of the dynamics based on an Euler method, including a Stokeslet derived interaction with a screening cutoff and a stochastic force accounting for Brownian and biogenic noise displays good agreement with the experimental results [30].

To quantify the self-organization, a Lempel-Ziv compression algorithm [31] is applied to each recorded image. As recently demonstrated [32], this algorithm, which is widely used in file compression applications, yields the computable information density (CID), f_C, which bounds the Shannon entropy [32] and is defined as

$$f_c \equiv \frac{\mathcal{L}(x)}{L}, \tag{2}$$

where $\mathcal{L}(x)$ is the length of a losslessly compressed string x and L is its uncompressed length. For nonequilibrium processes, traditional methods for characterizing order-disorder transitions often fail, and, in many instances, the order parameters are unknown. Nonetheless, the CID provides a generic measure of the order in the system without knowledge of the particular nature of the ordering. Simply compressing each successive microscopy image and recording the file size allows the determination of the experimental conditions under which the information

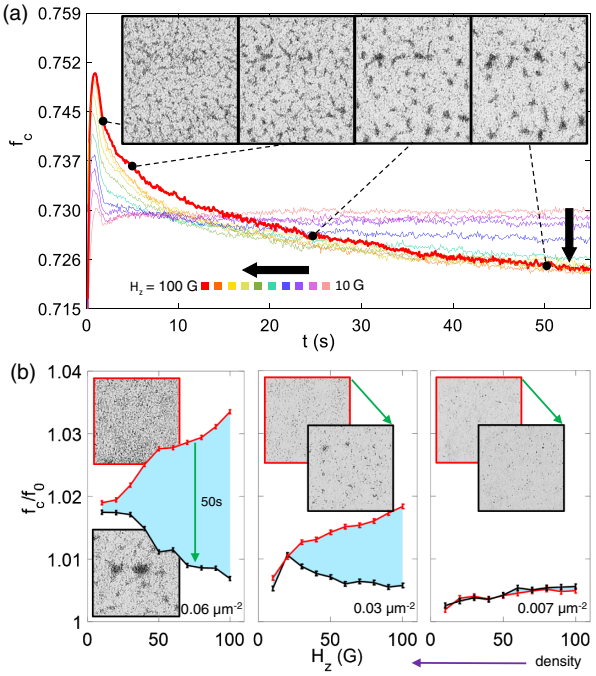

FIG. 2. (a) $f_c(t)$ for a population subjected to 10–100 G fields for 55 s (bold arrow indicates increasing magnetic field). The bolder, red curve shows the most dramatic drop in f_c under a 100 G field. As the field is decreased (other colors), the extent of the decay in f_c is reduced until at low values it remains nearly static in time. Inset: selected microscopy images from the self-organization process associated with the red (100 G) curve, taken at $t = 2.5$, 5, 25, and 50 s. (b) initial (red) and final (black) values of the scaled CID (f_c/f_0) as a function of field strength for various densities. As density decreases (left to right), the self-organization disappears at all field strengths (as seen in the decrease in the shaded area) Inset: selected images from 60 G field pulse showing initial (red outline) and final (black outline) representative configurations.

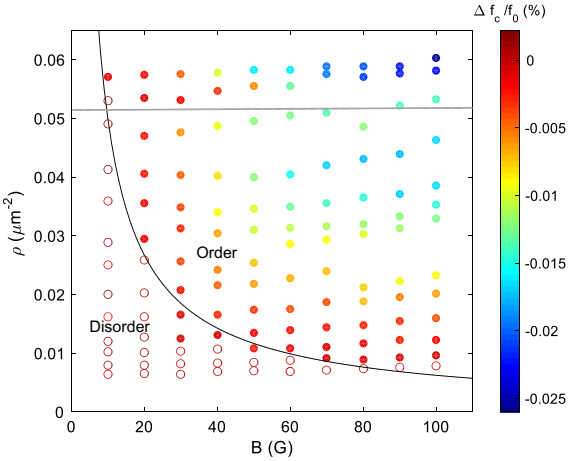

FIG. 3. Phase diagram illustrating the boundary between clustered states (closed circles) and disordered states (open circles). The color indicates the percentage drop in the scaled CID (f_c/f_0). The black line is a approximate power law fit to the phase boundary. The gray line indicates the threshold beyond which the density may not be reliably determined optically. Hence, for these points, the recorded density should be interpreted as a lower bound.

entropy drops in time. This allows a phase boundary to be constructed without explicitly identifying an order parameter.

To define the onset of self-organization, a pulsed field sweep is conducted. Figure 2 illustrates self-organization for a suspension observed in wide field (20× objective, see video S3 in Supplemental Material [19]). At $t = 0$, the field ($H_z = 10$–100 G) is turned on resulting in an initial rise in f_c. This transient (~1–2 s) results from the rapid increase in the number of oriented cells swimming towards the surface, as well as the finite reorientation time of cells already at the surface upon application of H_z. Once the cell density stabilizes (~2.5 s after H_z is introduced), f_c begins to decrease as self-organization proceeds. Figure 2(a) illustrates $f_c(t)$ for a sequence of 10 field strengths (at roughly constant density), each beginning from a random cell configuration. As the field strength is decreased, the decay of f_c with time is reduced until no significant reduction occurs over the interval. The gradual attenuation of the decay [Fig. 2(a)] indicates the disappearance of order as the magnetic field is reduced. It is noted that the structures themselves undergo dramatic qualitative changes ranging from uniform density ($t = 0$ s), filamentary networks ($t = 2.5$, 5.0 s) and isolated high density islands ($t = 25$, 50 s), for the high field (100 G) example depicted in Figs. 2(a) and 2 (inset).

To determine the effect of cell density on self-organization, pulsed field sweep (10–100 G) experiments were repeated over a range of densities. Between each field sweep, H_z is removed, allowing the cells to orientationally decohere and randomize their positions. Because cells swim freely in the zero-field state, a small fraction move out of the field of observation due to aerotaxis, leading to a continual reduction in the density (ρ). To track this decay, ρ is calculated directly from images by counting the cells (before each application of H_z), using ImageJ [33]. When the mean intercellular spacing in this disordered state approaches the optical size of the cells, this method no longer reliably measures the density at the surface and hence merely provides a lower bound (see Fig. 3).

To determine the presence of order at a given ρ and H_z, the change in f_c over a fixed time interval (55 s) is calculated. To compensate for density fluctuations within the interval, the initial and final values of f_c are respectively scaled by the zero-field CID (f_0), collected before and after application of the field. If the scaled value (f_c/f_0) drops more than the width of the noise in f_c/f_0 during the time the field is applied, we infer the presence of order.

Figure 2(b) shows the initial (red) scaled CID (f_c/f_0) plotted alongside its final (black) value for several field

sweeps at different densities. Figure 2(b) (left) is a high density case in which f_c/f_0 drops (shaded region) more than the noise at all measured field strengths. At a slightly lower density, Fig. 2(b) (center), the onset of self-organization only occurs when clear separation in f_c/f_0 is first evident at $H_z > 20$ G. As the density is further reduced, the order disappears entirely (as evidenced in the reduction in the shaded area) at even the highest magnetic field strengths [Fig. 2(b), right] indicating a low density of oriented cells.

Figure 3 summarizes results of 13 field sweeps conducted with the population corresponding to Fig. 2, which allows for the construction of a phase boundary separating ordered (open circles) from disordered states (closed circles). The color bar indicates the percentage drop in f_c/f_0 over the 55 s interval. Order disappears as the orientational coherence across the population is destroyed when H_z approaches zero. This decoherence occurs by the following: (i) the interplay between surface-induced hydrodynamic torques and the magnetic interactions that result in planar swimming [15,17] and (ii) an increase in the orientational noise [24]. Further, as ρ is reduced, stochastic forces begin to dominate the coherent hydrodynamic interactions when the timescale for attractive interaction becomes comparable to that of cell diffusion. As a result, the cells fail to attain an ordered state.

To understand the kinetics of the clustering process, the time evolution of the radial distribution function $g(r)$ (Fig. 4) is computed from the microscopy images. Initially ($t \sim 0.1$ s) $g(r)$ is largely flat, apart from a cutoff associated with the cell size. As clustering proceeds, a peak associated with cell-cell close packing separation distance grows and widens in time. The width of the peak is associated with the largest cluster dimension (~ 20 μm), while its area is proportional to the fraction of cells in the clustered state. An additional broad peak centered at an increasing separation distance is associated with the mean cluster-cluster distance. The probability of finding cells separated by larger distances (> 100 μm) is repressed relative to a random distribution (dashed line), corresponding with the distance between clusters and voids of reduced density.

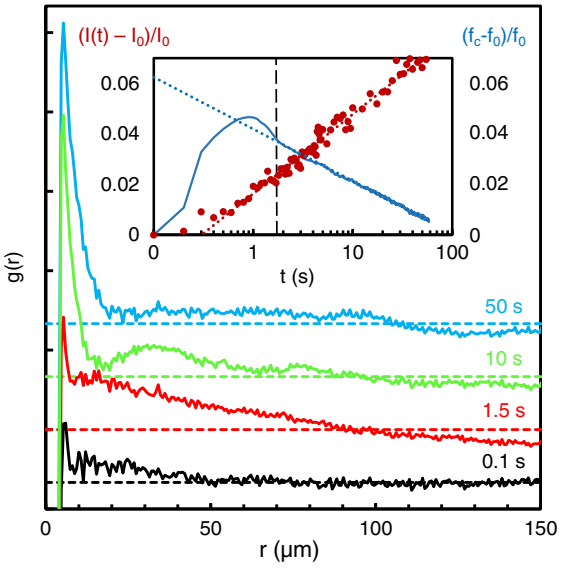

FIG. 4. $g(r)$, offset for clarity at $t = 0.1$, 1.5, 10, and 50 s after application of a 100 Oe external field (corresponding with the images in Fig. 2(a). The dashed line corresponds with the value of $g(r)$ expected for a noninteracting gas (a flat distribution). Inset shows a logarithmic increase in the peak associated with clustered cells (red) and the logarithmic scaling of the CID(blue) in time. Vertical dashed line indicates the onset of logarithmic scaling at $t \sim 2$ s after the initial transient.

Figure 4 (inset) shows the growth of the primary peak ($r \sim 5$ μm) area $I(t)$, relative to the area at the initial time I_0. After a transient (~ 1 s), the growth of the $I(t)$, and hence the size of the clusters, scales logarithmically in time. It has been previously shown both theoretically and experimentally that Brownian coalescence of monopolarly charged suspensions leads to logarithmic time dependence [34–36]. In these systems, particles come into contact through random collisions and stick through short-range contact forces (e.g., a van der Waals interaction). As the clusters accumulate charge, repulsion begins to suppress the growth rate. Similarly, in the present system, attractive hydrodynamic interactions are opposed by magnetic dipole-dipole repulsion. While the hydrodynamic attraction and magnetic repulsion are both predicted to have the same long range asymptotic behavior ($\sim 1/r^4$), the hydrodynamic effects experience an effective cutoff, due to screening and stochastic effects. The hydrodynamic forces are of greater strength at μm range ($\sim$pN) relative to the magnetostatic forces (~ 0.01 pN, for magnetic moments $\sim 10^{-16}$ A m^2 [24]) for pairs of cells. However, as the clusters grow and increase in total magnetic moment, the magnetic forces become comparable to the hydrodynamic forces. Thus, the structure and logarithmic kinetics of the clusters may be understood as an interplay between attractive hydrodynamics with a finite range and repulsive magnetic interactions that scale with the cluster size, thereby inhibiting the continued rapid growth of the clusters. In this sense, the process may be understood as an active matter analog to the self-focusing regime in passive charged colloids [34]. Interestingly, as shown in Fig. 4 (inset) the CID also scales logarithmically in time after an initial transient ($t \sim 1$ s). This suggests a direct physical interpretation of the CID as providing information about the configurational entropy of the cells, which decreases as they coalesce, and are constrained to occupy a smaller volume.

In conclusion, we have shown that when oriented near a surface, AMB-1 experience attractive hydrodynamic interactions arising from their flagellar activity, which are well captured by a simple analytical model based on a pure Stokeslet and its image system. Moreover, these interactions along with dipolar magnetic repulsion, give rise to

spontaneous, self-organized bacterial clusters where the CID (which bounds the Shannon entropy) reveals the phase boundary defining the onset of self-organization. Kinetics of cluster growth are governed by the interplay between hydrodynamic attractive forces and magnetic repulsion, analogous to the self-focusing of charged inactive colloids. Taking advantage of the high degree of experimental control and theoretical tractibility of the present system, future studies should address broad questions in non-equilibrium active self-organization. Particularly salient are questions regarding the specific nature of the ordering and what critical behavior, if any, accompanies the onset of self-organization. Additionally, the thermodynamic implications of the relationship between dissipation and structure formation in active systems should be explored.

This material is based upon work supported by the National Science Foundation under Grants No. ECCS 1710598 and EAR-1424138. We also thank Ciriam Jayaprakash for useful discussions.

[1] E. Mehes and T. Vicsek, Integr. Biol. **6**, 831 (2014).
[2] A. Sokolov and I. S. Aranson, Phys. Rev. Lett. **109**, 248109 (2012).
[3] C. R. Reid, M. J. Lutz, S. Powell, A. B. Kao, I. D. Couzin, and S. Garnier, Proc. Natl. Acad. Sci. U.S.A. **112**, 15113 (2015).
[4] W. Bialek, A. Cavagna, I. Giardina, T. Mora, E. Silvestri, M. Viale, and A. M. Walczak, Proc. Natl. Acad. Sci. U.S.A. **109**, 4786 (2012).
[5] J. Palacci, S. Sacanna, A. P. Steinberg, D. J. Pine, and P. M. Chaikin, Science **339**, 936 (2013).
[6] W. Wang, W. Duan, S. Ahmed, A. Sen, and T. E. Mallouk, Acc. Chem. Res. **48**, 1938 (2015).
[7] M. Rubenstein, A. Cornejo, and R. Nagpal, Science **345**, 795 (2014).
[8] S. Ramaswamy, J. Stat. Mech.-Theory E. **2017**, 054002 (2017).
[9] M. C. Marchetti, J. F. Joanny, S. Ramaswamy, T. B. Liverpool, J. Prost, Madan Rao, and R. Aditi Simha, Rev. Mod. Phys. **85**, 1143 (2013).
[10] C. Lefevre and D. Bazylinski, Microbiol. Mol. Biol. Rev. **77**, 497 (2013).
[11] S. Martel, C. Tremblay, S. Ngakeng, and G. Langlois, Appl. Phys. Lett. **89**, 233904 (2006).
[12] O. Felfoul, M. Mohammadi, S. Taherkani, D. de Lanauze, Y. Xu, D. Loghin, S. Essa, S. Jancik, D. Houle, M. Lafleur, L. Gaboury, M. Tabrizian, N. Kauo, M. Atkin, T. Vuoung, G. Batists, N. Beuchemin, D. Radzioch, and S. Martel, Nat. Nanotechnol. **11**, 941 (2016).
[13] L. Gonzalez, W. C. Ruder, P. Leduc, and W. Messner, Sci. Rep. **4**, 4104 (2015).
[14] J. Loehr, D. Pfeiffer, D. Schuler, and T. Fischer, Soft Matter **12**, 3631 (2016).
[15] C. J. Pierce, E. Mumper, E. E. Brown, J. T. Brangham, B. H. Lower, S. K. Lower, F. Y. Yang, and R. Sooryakumar, Phys. Rev. E **95**, 062612 (2017).
[16] G. Vieira, T. Henighan, A. Chen, A. J. Hauser, F. Y. Yang, J. J. Chalmers, and R. Sooryakumar, Phys. Rev. Lett. **103**, 128101 (2009).
[17] A. P. Berke, L. Turner, H. C. Berg, and E. Lauga, Phys. Rev. Lett. **101**, 038102 (2008).
[18] K. Drescher, K. C. Leptos, I. Tuval, T. Ishikawa, T. J. Pedley, and R. E. Goldstein, Phys. Rev. Lett. **102**, 168101 (2009).
[19] See Supplemental Material at http://link.aps.org/supplemental/10.1103/PhysRevLett.121.188001 for videos of a pair of cells coming together and rotating (S1), a small cluster of cells coalescing (S2), and a wide-field image of a dense suspension under the influence of 100 Oe field. See also videos S2 and S3.
[20] S. Kim and S. Karilla, *Microhydrodynamics: Principles and Selected Application* (Dover, New York, 2005).
[21] E. Lauga and T. R. Powers, Rep. Prog. Phys. **72**, 096601 (2009).
[22] S. Spagnolie and E. Lauga, J. Fluid Mech. **700**, 105 (2012).
[23] T. Squires, J. Fluid Mech. **443**, 403 (2001).
[24] R. Nadkarni, S. Barkley, and C. Fradin, PLoS One **8**, e82064 (2014).
[25] M. Hughes and H. Morgan, Biotechnology Progress **15**, 245 (1999).
[26] N. Darnton, L. Turner, S. Rojevsky, and H. Berg, J. Bacteriol. **189**, 1756 (2007).
[27] S. Chattopadhyay, R. Moldovan, C. Yeung, and X. Wu, Proc. Natl. Acad. Sci. U.S.A. **103** (2006).
[28] A. P. Petroff, X.-L. Wu, and A. Libchaber, Phys. Rev. Lett. **114**, 158102 (2015).
[29] X. Chen, X. Yang, M. Yang, and H. P. Zhang, Europhys. Lett. **111**, 54002 (2015).
[30] C. J. Pierce, H. Wijesinghe, and R. Sooryakumar (to be published).
[31] J. Ziv and A. Lempel, IEEE Trans. Inf. Theory **23**, 337 (1977).
[32] S. Martiniani, P. M. Chaikin, and D. Levine, arXiv:1708.04993.
[33] J. Schindelin, I. Arganda-Carreras, E. Frise, V. Kaynig, M. Longair, T. Pietzsch, S. Preibisch, C. Rueden, S. Saalfeld, J. Schmid, B. Tinevez, D. J. White, V. Hartenstein, P. Eliceiri, and K. Tomancak, Nat. Methods **9**, 676 (2012).
[34] S. M. Dammer and D. E. Wolf, Phys. Rev. Lett. **93**, 150602 (2004).
[35] K. Roger, R. Botet, and B. Cabane, Langmuir **29**, 5689 (2013).
[36] R. Botet and K. Roger, Curr. Opin. Colloid Interface Sci. **22**, 108 (2016).

Correction: Two references and their citations in text were missing and have been inserted. Three incorrect figure citations in text have been fixed. Errors in the author list and arXiv number in Ref. [32] have been straightened out.